Journal of Computational Electronics
https://doi.org/10.1007/s10825-021-01687-7

A new analytical model for the response of AlGaN/GaN HEMT-based pH sensors

Kavita Thorat Upadhyay[1,2] · Manju K. Chattopadhyay[3]

Received: 22 October 2019 / Accepted: 6 March 2021

Abstract
pH sensors are monitoring devices with wide applications in biology, chemistry, medicine, and agriculture. To enhance their sensitivity and long-term stability, efficient study of such devices becomes imperative but is impossible without the aid of accurate analytical models. A new analytical model for the pH sensing characteristics of AlGaN/GaN-based high-electron-mobility transistors (HEMTs) is presented herein, as well as theoretical predictions and optimization of the charge sensitivity for ungated AlGaN/GaN HEMT-based pH sensors. The change in the drain current with the changing surface potential due to a variation in the pH of the electrolyte is calculated for devices with different Al mole fractions, AlGaN thicknesses, gate length spacings, and passivation layers. The numerical values for the drain current, threshold voltage, and surface potential obtained by using this new model show good agreement with available experimental results. It is demonstrated that the sensitivity of GaN HEMT-based pH sensors at lower pH values can be improved by applying a SiN_x passivation layer to the HEMT. The calculated average root-mean-square error of our model is 0.018, being an order of magnitude lower than other models reported in literature.

Keywords GaN HEMT · 2DEG · Analytical model · Chemical sensor · pH sensing · Sensitivity

1 Introduction

The normal range of pH variation for human blood is 7.35–7.45. Any deviation in the pH value of a biomolecule may indicate a disease, possibly with severe effects [1]. pH measurement is also vital in many other fields including biomedicine, food and nutrition, ecological studies, chemistry, and oceanography. Electrochemical (EC) liquid sensors thus find application in numerous biomedical practices [2]. The absence of a gate electrode makes ion-sensitive field-effect transistor (ISFET)-based sensors an important type of EC sensor for measuring pH [3, 4]. However, since the gate region in an ISFET is prone to charging effects, a reference electrode must be used to bias the gate area to above the threshold voltage and thus allow a drain current flow. High-electron-mobility transistors (HEMTs), on the other hand, do not need a gate voltage to turn on.

A suitable choice of sensing material is as important as the device selection. During the last three decades, substantial efforts have been made towards the development of novel semiconductor materials exhibiting physical and mechanical properties that can overcome the fundamental limits of silicon-based conventional electronics, which are mature and less expensive. Among these materials, wide-bandgap (WBG) semiconductors such as silicon carbide (SiC) [5, 6], diamond [7–9], and gallium nitride (GaN) have been shown to possess superior properties [10]. SiC and GaN are the most well-known WBG devices, offering attractive features that make them suitable for operation in high-temperature conditions, such as a wide bandgap (3 eV), high drift saturation velocity, high thermal conductivity, low intrinsic carrier concentration, and large critical electric field. Both GaN and SiC belong to the same family of WBG semiconductors and share similar, attractive properties. SiC has attracted great attention for use in high-temperature applications [11].

✉ Manju K. Chattopadhyay
mkorwal@yahoo.com

[1] Department of Electronics and Communication Engineering, IPS Academy, Institute of Engineering and Science, Indore 452012, India

[2] Department of Electronics and Telecommunication Engineering, Institute of Engineering and Technology, Devi Ahilya University, Indore 452017, India

[3] School of Electronics, Devi Ahilya University, Khandwa Road, Indore 452017, India

Published online: 29 March 2021

However, most work reported in this field has been realized with either large areas or low device density integration. The direct temperature dependence of the carrier concentration, due to the bulk nature of the active region in SiC devices, is a known shortcoming of SiC [12]. Moreover, at higher temperatures, the junction leakage of SiC devices is degraded due to crystal dislocations. GaN offers a considerable performance improvement over SiC with respect to the response speed, operating temperature limits, and reverse recovery characteristics [12]. At low breakdown voltages, GaN devices offer lower channel resistance than SiC devices. Owing to its comparatively better physical and chemical stability, GaN is also an ideal material for the development of explicit chemical sensor and biosensor systems [13]. A detailed review on significant research work in the field of sensor technology based on GaN heterostructures can be found in our recent work [14].

AlGaN/GaN HEMTs have become popular for use in high-frequency radiofrequency (RF) power amplifier and power switching applications as well [15]. Their high sheet carrier concentration derives from the polarization-induced two-dimensional electron gas (2DEG) produced at the AlGaN–GaN interface. The density of the 2DEG is balanced by the surface charge state. The sheet charge density in the 2DEG channel is thus very sensitive to the charge on the AlGaN surface. The strong chemical stability and the WBG of group III N materials ensure that such AlGaN/GaN heterostructures can operate as chemical sensors in harsh acidic or alkaline environments and at very high temperatures. In particular, these chemical sensors can be incorporated into biosystems because of their biological compatibility and nontoxicity. This has provided the foundation for new acute medical care systems in recent years [16, 17].

As stated above, pH measurement is a major consideration in almost all fields involving chemicals. pH monitoring is also required for seawater analysis, for soil analysis to check its fertility, and in the food processing industry. pH also plays a decisive role in targeted drug release from nanoscale drug carriers. Based on these applications, pH measurement has become an extremely important topic for researchers working in diverse fields [18].

1.1 The sensing mechanism

An electrolyte solution with different pH values can be considered to represent a type of intrinsic semiconductor material because the mobile ions in solution are similar to electron and hole charges in semiconductors. The pH sensing mechanism is related to reactions between ions in the electrolyte solution with different pH values and the positive surface charge induced by the polarization on the surface of HEMTs. A probable mechanism for the adsorption of positive and negative charges that change the potential at the AlGaN/Au and Au/electrolyte interfaces related to the H^+ concentration is explained by the site binding model introduced by Yates et al. and Munch et al. [19, 20]. In this model, hydroxyl groups at the surface act as amphoters. They may be dependent on the H^+ concentration and the equilibrium constants for the related reactions:

$$\mathrm{MOH} \leftrightarrow \mathrm{MO}^- + \mathrm{H}^+ \tag{1}$$

$$\mathrm{MOH} + \mathrm{H}^+ \leftrightarrow \mathrm{MOH}_2^+ \tag{2}$$

Here, M is either Si or a metal in MOH. Because of the formation of more protonized hydroxyls MOH_2^+, the 2DEG concentration increases to balance the positive charge induced on the surface. Vice versa, negative charges at the insulator surface decrease the H^+ concentration in solution. A high sensitivity of GaN-based pH sensors to hydronium ions was reported in Ref. [21]. The sensitivity S of such sensors can be regarded as capturing the modification of the surface potential ψ_0 as a function of the concentration of hydronium ions in the electrolyte.

In different electrochemical and non-electrochemical methods used for measuring pH, AlGaN/GaN HEMTs have shown great promise for achieving unprecedented speed and sensitivity. Indeed, GaN-based pH sensors showed high sensitivity of 57.3 mV/pH to hydronium ions [22, 23]. The sensitivity of these sensors is related to the action between ions in the electrolyte on the open region of the device and the positive surface charge induced by polarization. This action causes a change in the surface charge on the devices. Non-modulation-doped GaN HEMTs have been investigated due to their advantages such as a reduced gate leakage current, lower $V_{\text{pinch-off}}$ value, and lower noise due to the absence of donors from the AlGaN layer [24, 25].

Stutzmann et al. [26] and Mehandru et al. [27] reported preliminary results on the response of open-gate AlGaN/GaN HEMTs to polar liquids. Kokowa et al. first experimentally investigated the pH-sensing characteristics of unpassivated u-AlGaN/GaN HEMT structures [28]. Later, Abidin et al. [24] investigated the surface of the open gate of an HEMT experimentally. An increase in the pH level leads to a shift of the threshold voltage towards the positive side.

Sharma et al. verified the characteristics of a pH and salinity sensor fabricated using gated AlGaN/GaN HEMT structures in phosphate buffer saline (PBS) and aqueous salt solutions [29]. In deionized (DI) water, the HEMT devices displayed I_d–V_d characteristics similar to the output characteristics of classical HEMT structures in air. A sensitivity of 6.48 mA/mm-molar and a response time of 250–350 ms at $V_{ds} = +1$ V were obtained using these GaN HEMT structures [29]. Cheng et al. demonstrated a pH sensor based on a planar dual-gate AlGaN/GaN HEMT cascode amplifier that enhanced the pH sensitivity by about 45 times from

45 mV/pH to 2.06 V/pH with linearity of 1.27% [30]. Xue et al. illustrated how to adjust the threshold voltage V_T of an AlGaN/GaN HEMT-based pH sensor from −3.46 to −1.15 V by applying photo-electrochemical (PEC) oxidation on the GaN cap layer surface. They postulated that the sensitivity of this reference electrode sensor could be considerably improved by varying the V_T value so that $V_G|g_{mMAX}$ would approach the corresponding gate voltage when a droplet is placed on the sensing window plane. This approach may be beneficial for scaling down and integration of future AlGaN/GaN HEMT pH sensors [31].

Zhang et al. theoretically and experimentally investigated the result of varying the gate geometry of a pH sensor on its sensitivity. The series resistance (R_S) of the packaged sensor was found to be an important feature limiting the current sensitivity. They found an optimum for $W/L = \rho_{(2DEG)}/R_S$ [32].

1.2 The analytical model

Since the formation of the 2DEG determines the drain current flowing in a HEMT device, an accurate physics-based analytical expression for the 2DEG electron sheet concentration (n_s) is a prime necessity for developing a model for such devices. The main complexity in analytical modeling of the 2DEG electron sheet concentration (n_s) is its subtle variation with the applied voltage.

Several theoretical–mathematical models for the drain *I–V* characteristics of AlGaN/GaN HEMT devices have been reported in literature [33–40], among which the model described by Toufik et al. [34] is one of the most popular. This is an empirical method that uses a large number of fitting parameters that must be extracted from experimental data. However, physics-based models are preferred for better prediction of the statistical variations in the device [35]. They follow well-defined geometrical and temperature scaling rules [36–39]. Khandelwal et al. [41] proposed a model for n_s based on only the first quantum energy level E_0 of the conduction band of GaN. That model does not account for the electron concentration in the AlGaN layer and uses an interpolation function for n_s. Karumuri et al. [42] divided the operating zone of the HEMT into three regions depending on the relative position of the Fermi level E_F: region 1 for $E_F < E_0$, region 2 for $E_0 < E_F < E_C$, and region 3 for $E_F > E_C$. In region 3, the E_F crosses the conduction-band minimum of AlGaN at the interface. The electron concentration in the AlGaN barrier layer (n_B) thus also becomes important for the accuracy of the 2DEG model. Both Karumuri et al. [43] and Swamy et al. [43] developed models using simplified Fermi–Dirac statistics. Swamy et al. [43] proposed a model for n_s that does not need an interpolation function and uses only four fitting parameters. In contrast, the model developed by Khandelwal et al. [41] uses two interpolation functions. The accuracy level of the model proposed by Swamy et al. [43] is comparable to that of Karumuri et al. [42].

Rabbaa et al. [44] applied a basic theoretical model to calculate the 2DEG electron sheet concentration (n_s) and the drain current in the HEMT as well as the surface potential due to the pH of the electrolyte solution. However, their model uses iterative techniques that are unsuitable for circuit simulations. Their method of calculating the saturation velocity requires excessive computation, too. Their model suffers from the additional limitation that the parameters used must be fine-tuned by approximately 5% to obtain a perfect match with experimental results.

To overcome the above-mentioned problems, we modified the model for n_s proposed by Swamy et al. [43] for quaternary alloy AlInGaN/GaN HEMTs and obtained a satisfactory match of the results with experimental data [45]. In the present work, we extend this modified model to make it applicable for the investigation of pH sensing applications using AlGaN/GaN HEMTs, making the following changes:

(i) The electron concentration n_B in the AlGaN barrier layer is also included in the unified model of Ref. [43]. Here, since we are analyzing a model for pH sensors operating in the region with $E_F < E_c$ and with a negligible n_B, we use the model only for n_s but deliberately neglect n_B, resulting in a simplified model. Thus, our parameters are chosen different from those in Swamy's model.
(ii) Iterative techniques are not used to calculate the surface potential caused by the pH of the electrolyte solution.
(iii) The values of the parameters are not approximated as done by Rabbaa et al. [44]. We use suitable fitting parameters without approximation.
(iv) The model of the drain current is not divided into regions, unlike that of Rabbaa et al. [44], thus simplifying it further.
(v) The current model is implemented specifically for AlGaN/GaN pH sensors.

The results calculated using the new model show good agreement with experimental results reported in literature. This paper is organized as follows: Sect. 2 discusses the device structure. Sections 3.1, 3.2, and 3.3 present the basis for our model for n_s and the charge-based current models. Section 3.4 introduces the model for the surface potential. Section 4 presents the results, while conclusions are drawn in Sect. 5.

2 The device structure

A cross-sectional view of the AlGaN/GaN HEMT device structure is shown in Fig. 1. This structure consists of a thick GaN buffer layer with a width of about 1–2 μm and

an AlGaN barrier layer with a typical thickness ranging between 10 and 30 nm. The gate bias can be applied at the open-gate area through a saturated calomel electrode (SCE), which is the reference electrode having a well-defined stable potential that is not affected by the concentration of hydrogen ions in the sample solution. To measure the pH value, the device along with the SCE is placed into an electrochemical cell filled with electrolyte solution [28].

Conducting channels form in the HEMTs due to the conducting layer of free electrons at the heterointerface between the doped wide-bandgap semiconductor (AlGaN) and the undoped narrower-bandgap semiconductor (GaN). Electrons from the edge region of the doped AlGaN are transferred into the lower-bandgap GaN semiconductor and collect in the quantum well that forms in the GaN at the junction of the two materials. The electrons are confined in the quantum well and are known as a 2DEG. The 2DEG is located in the region of undoped GaN, where the carrier mobility is high due to the reduced scattering effect. The 2DEG offers the advantage that there are no impurity atoms in the undoped GaN quantum well. Changes in the heterojunction space result in changes in the 2DEG concentration, thereby affecting the source–drain current. Due to the high carrier concentration, high electron mobility, and wide bandgap, such HEMT devices are sensitive to noise and even small variations in the current magnitudes.

3 A description of the model

It has been established that the formation of a 2DEG in the heterostructure is the most important effect of the polarization property of nitride alloys. Literature presents many useful predictions based on theoretical and experimental studies of the polarization property of ternary AlGaN alloys. For the AlGaN/GaN HEMT, the threshold voltage V_{th} is related to the polarization as [44],

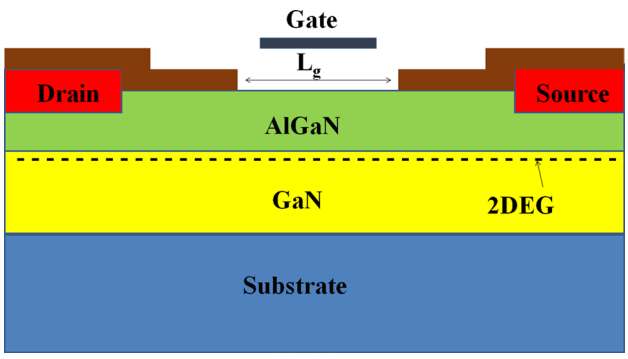

Fig. 1 A cross-sectional view of the open-gate AlGaN/GaN HEMT dipped in an electrolyte. The gate bias is applied through the gate electrode to the electrolyte–AlGaN interface

$$V_{\text{th}} = \frac{\varnothing_{\text{b}}}{q} - \frac{\Delta E_{\text{c}}}{q} - \frac{qn_{\text{d}}d^2}{2\varepsilon} - \frac{q\sigma_{\text{int}}d}{\varepsilon} \tag{3}$$

where $\varnothing_{\text{b}}$ is the height of the Schottky barrier, ΔE_{c} is the conduction-band discontinuity, q is the electron charge, n_{d} is the doping concentration, ε is the permittivity of the material, d is the thickness of the AlGaN layer, $\sigma_{\text{int}} = P_{\text{GaN}} - P_{\text{AlGaN}}$ where P_{GaN} is the polarization of GaN and P_{AlGaN} is the polarization of AlGaN, given by the sum of the spontaneous and piezoelectric polarizations:

$$P_{\text{AlGaN}} = P_{\text{sp}}(\text{AlGaN}) + P_{\text{pz}}(\text{AlGaN}) \tag{4}$$

3.1 The carrier density model

The sheet charge density n_{s} of the 2DEG as a function of position x in the channel can be obtained by solving the one-dimensional Poisson equation and is given as [44]:

$$n_{\text{s}} = \frac{\varepsilon}{qd_{\text{i}}}\left(V_{\text{g}} - V_{\text{th}} - V_{y} - \frac{E_{\text{F}}}{q}\right), \tag{5}$$

where d_{i} is the total length of the AlGaN and GaN layer, V_{g} is the gate voltage, V_{y} is the channel potential at a distance y, and E_{F} is the Fermi level.

As mentioned above, the current model is used to analyze an AlGaN/GaN heterostructure operating as a pH sensor in the region $E_{\text{F}} < E_{\text{c}}$, where the electron concentration in the AlGaN layer n_{B} is negligible. Hence, only n_{s} is used in the model while n_{B} is neglected. n_{s} can be expressed analytically as a function of V_{g} thus [45]

$$n_{\text{s}} = \frac{AV_{\text{go}}}{(1+B)}\left(\frac{1 - A^{\frac{2}{3}}\gamma_0}{(1+B)^{\frac{2}{3}}V_{\text{go}}^{\frac{1}{3}}}\right), \tag{6}$$

where $V_{\text{go}} = V_{\text{g}} - V_{\text{th}}$, $A = \varepsilon/qd$, $B = A/qD$, D is the density of states, and γ_0 is a constant estimated from Shubnikov–De Haas or cyclotron resonance experiments.

3.2 The charge-based drain current model

An analytical model for the current is formulated using the definition of the drain current along the channel given by

$$I_{\text{D}} = q\mu W\left[n_T\left(\frac{\text{d}V_y}{\text{d}y}\right) - \left(\frac{kT}{q}\right)\left(\frac{\text{d}n_T}{\text{d}y}\right)\right], \tag{7}$$

$$\text{d}V_y = -\text{d}n_T\left(\frac{A+D}{AD} + \frac{2}{3}\gamma_0 n_T^{\frac{-1}{3}}\right), \tag{8}$$

where W is the width, μ is the low-field mobility of the device, n_T is the sheet carrier density in the channel that

contributes to current conduction at any given distance y, k is the Boltzmann constant, and T is the ambient temperature. Taking the limit of y from the source to drain and integrating Eq. 7 yields the following expression for the drain current:

$$I_D = \frac{q\mu_{eff}W}{L_g}\left[\frac{A+D}{2AD}\left(n_s^2 - n_D^2\right) + \frac{2}{5}\gamma_0\left(n_s^{\frac{5}{3}} - n_D^{\frac{5}{3}}\right) + \frac{kT}{q}\left(n_s - n_D\right)\right], \tag{9}$$

where n_s and n_D are the charge carrier concentration at the source and the drain, respectively. μ_{eff} is the effective 2DEG mobility, and L_g is the gate length. n_s here is calculated using Eq. (6). The calculation of n_D is explained in the next section.

3.3 The saturation voltage

The saturation voltage is modeled using the approach given in Ref. [46]:

$$V_{sat} = \frac{v_s V_{go}}{v_s + \frac{\mu_{eff} V_{go}}{2L}}, \tag{10}$$

where v_s is the saturation velocity. The above Eq. (10), commonly used in many metal–oxide–semiconductor field-effect transistor (MOSFET) models, is adopted here for the case of HEMTs to obtain the effective mobility as [46]

$$\mu_{eff} = \frac{\mu_0}{\left(1 + a_1 V_{go} + a_2 V_{go}^2\right)\left(1 + a_3 V_{ds}\right)}, \tag{11}$$

where a_1, a_2, and a_3 are fitting parameters.

Once the saturation voltage is calculated, the effective drain voltage $V_{eff,D}$ can be obtained. $V_{eff,D}$ is designed to achieve a smooth transition between the applied drain–source voltage V_{ds} and the saturation voltage V_{sat} [43]:

$$V_{eff,D} = V_{sat}\left[1 - \frac{\ln\left[1 + exp(1 - \alpha\frac{V'_{ds}}{V_{sat}})\right]}{\ln(1+e)}\right], \tag{12}$$

where α is the transition width parameter and V'_{ds} represents the effective drain–source voltage under the calculated by subtracting the voltage drops due to the resistances at the source and drain from the drain–source voltage. The charge carrier concentration at the drain n_D is calculated using Eq. (6) by replacing V_{go} with $V_{gdo} = V_{go} - V_{eff,D}$. As mentioned above, for pH sensing applications, only the sheet charge carrier concentration n_s need be considered but not n_B. Hence, the values of the fitting parameters in our model are different from those of Ref. [43]. This makes our model simpler, too. The values of these parameters are taken as presented in Table 1, calculated for three different devices to compare the results presented herein with various experimental data and thereby validate the model. All the parameters for device 1 are the same as in Ref. [43] except for the transition width parameter α.

3.4 pH sensing

HEMTs show significant sensitivity to relatively small changes in the pH level of a liquid. When the surface of a HEMT is exposed to an electrolyte solution with a specific concentration, the change in the surface charge and potential causes a change in the channel charge density, which further modulates the drain current. This mechanism can be used to build a sensor to measure the pH of the solution.

Therefore, the effect of the electrolyte solution on the device manifests in the potential [47], as follows:

$$\psi_0 = -\log_e 10\delta_t V_{th}(\mathrm{pH} - \mathrm{pH}_{PZC}), \tag{13}$$

where $\delta_t = \frac{\gamma}{1+\gamma}$, $\gamma = \frac{qN_{ss}\eta}{C_{eq}V_{th}}$, $\eta = 2 \times 10^{-\frac{(pK_b - pK_a)}{2}}$, $C_{eq} = \frac{C_{DL}C_{Stern}}{C_{DL}+C_{Stern}}$, $C_{DL} = \frac{\sqrt{8\varepsilon V_T q n_0}}{2V_{th}}$, $\mathrm{pH}_{PZC} = \frac{pK_a + pK_b}{2}$. Here γ is defined by the Gouy–Chapman Stern model [47], C_{Stern} is the capacitance of the Stern layer ($C_{Stern} = 20\ \mu F/cm^2$) [47], n_0 is the ionic charge concentration in the electrolyte, V_T is the thermal voltage, and N_{ss} is the site binding charge, given in Table 2.

The surface potential ψ_0 is subtracted from the threshold voltage to obtain the effective threshold voltage V_{eth}, represented as [44]

$$V_{eth} = V_{th} - \Psi_0. \tag{14}$$

This effective threshold V_{eth} replaces the threshold voltage V_{th} in all the calculations.

4 Results

To validate the model, the results are compared with the experimental data for device 1 reported in Ref. [48]. Device 1 has a gate length of 1 µm and a gate width of 75 µm. The Al mole fraction is 15% in the 25-nm AlGaN layer of device 1. Figure 2 depicts the drain current versus the gate voltage to compare the values calculated using the presented model, those calculated using the model introduced in Ref. [43], and the experimental data from Ref. [48]. The results show that all three sets of results match very well for $V_d = 5$ V, even though our model has fewer parameters than that described in Ref. [43] and n_B is excluded as well.

The surface potential is calculated for two surfaces of the HEMT. The first is the bare AlGaN surface, while the second one is an SiN_x-covered AlGaN surface. An unintentional thin oxide layer forms on the exposed AlGaN surface when

Table 1 The parameter values used in the model for fitting and for various aspects of the device design

Parameter (units)	Given in Ref. [43] for device 1	The model parameters		
		Device 1	Device 2	Device 3
Depicted in	[43]	Figure 2	Figures 5 and 6	Figures 7 and 8
Al mole fraction in AlGaN (dimensionless)	0.15	0.15	0.23	0.25
AlGaN layer thickness (nm)	25	25	22	25
Gate length (μm)	1	1	10	40
Gate width (μm)	75	75	500	490
V_{off} (V)	−2.9	−2.9	−4.9	−6.1
Low-field mobility, μ_0 (cm^2/V-s)	600	600	950	1860
Fitting parameter, a_1 (1/V)	5.5×10^{-3}	5.5×10^{-3}	10	60×10^{-3}
Fitting parameter, a_2 ($1/V^2$)	1.5×10^{-3}	1.5×10^{-3}	0.05	15×10^{-3}
Fitting parameter, a_3 (1/V)	2×10^{-3}	2×10^{-3}	0.34	0.001
Source–gate region resistance, R_s (Ω)	0.72	0.72	0.45	0.75
Drain–gate region resistance, R_d (Ω)	0.72	0.72	0.45	0.75
Transition width parameter, α (dimensionless)	0.01	0.32	0.82	1

Table 2 The site-binding parameters of different passivation layers [47]

Passivation layer	ε	pK_a	pK_b	N_{ss}
SiN_x	7.5	−2	6	3×10^{14} cm^{-2}
Ga_2O_3	10.2	4.81	10.91	3×10^{14} cm^{-2}

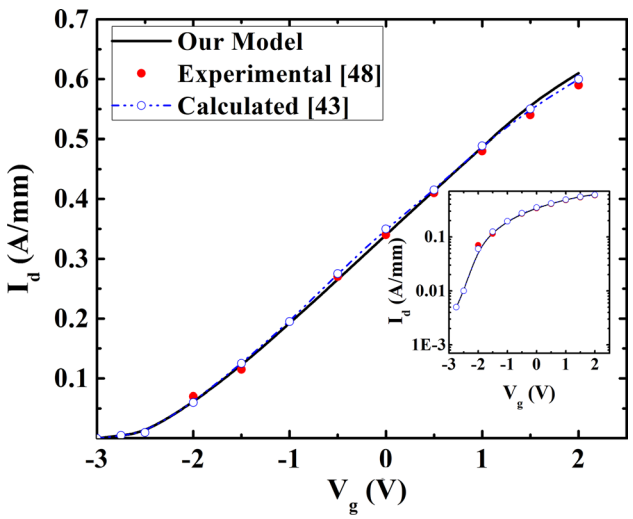

Fig. 2 The drain current I_d versus the gate voltage V_g for a drain voltage of $V_d = 5$ V, enabling a comparison of the results calculated herein with the experimental data in Ref. [48] for device 1 and the theoretical results obtained using the model described in Ref. [43]. The inset shows the same data plotted on a logarithmic scale. Solid dots represent the experimental data, while hollow symbols with dotted lines show the data calculated using the model described in Ref. [43], and continuous lines represent the calculations using the model described herein

it comes into contact with air [44]. This unintentional Ga_2O_3 layer changes the surface potential. This effect is calculated by considering the parameters related to Ga_2O_3 [44].

Figure 3 shows the variation of the surface potential with the change in the pH value for Ga_2O_3 and the SiN_x layer on the AlGaN surface of the HEMT. The results calculated for Ga_2O_3 and SiN_x match with the experimental results given by Rabbaa et al. [44] and Kokawa et al. [28], respectively. The surface potential decreases linearly with the pH value from 2 to 12.

A change in the surface potential causes a shift in the threshold voltage, which affects the sensitivity of the device. The device sensitivity is defined as

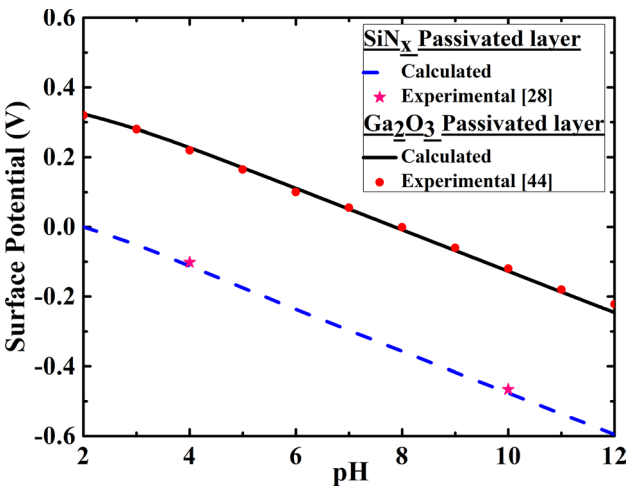

Fig. 3 The variation of the surface potential with the pH value, illustrating the agreement of the calculations using the present model, for SiN_x and Ga_2O_3 passivation layers, with the experimental results presented in Ref. [28] and [44], respectively

$$\text{sensitivity} = \frac{V_{\text{thpH1}} - V_{\text{thpH2}}}{\text{pH1} - \text{pH2}} = \frac{\Delta V_{\text{th}}}{\Delta \text{pH}}. \quad (15)$$

Figure 4 shows the variation in the sensitivity of the device with different passivation layers, viz. SiN_x and Ga_2O_3. The results of the present calculations show that, for SiN_x and Ga_2O_3 layers, the maximum sensitivity is 0.062 V/pH and 0.060 V/pH while the average sensitivity is 0.595 V/pH and 0.058 V/pH, respectively. The sensitivity is approximately equal to the Nernstian response, i.e., 0.59 V/pH. Kokawa et al. [28] reported an experimental pH sensitivity of 0.0567 V/pH with an SiN_x layer. We also infer here that the change in the threshold voltage of the device is higher for pH < 7, i.e., for acidic solutions, while the sensitivity is lower for basic solutions. We observe that the device with an SiN_x passivation layer is more sensitive than the device with a Ga_2O_3 layer for acidic solutions.

Figures 5 and 6 depict the I_d–V_g characteristics of HEMT device 2 when covered with electrolyte solution of different pH values. Device 2 is an SiN_x-layered HEMT with an Al mole fraction of 23%, a 22-nm-thick AlGaN layer, a gate length of 10 µm, and a gate width of 500 µm. Figure 5 compares the results with the experimental results of Kokawa et al. [28] and the theoretical results obtained using the I_d model proposed by Rabbaa et al. [44]. The values calculated herein at $V_{ds} = 0.2$ V for different pH values are in good agreement with the experimental results of Kokawa et al. [28]. It can be observed that the results of our model provide a better match than those of Ref. [44] without requiring any approximation in the parameters. The curves represent the results calculated using our model, while the symbols in the graph denote the experimental results of Kokawa et al. The calculated results match well with the experimental data

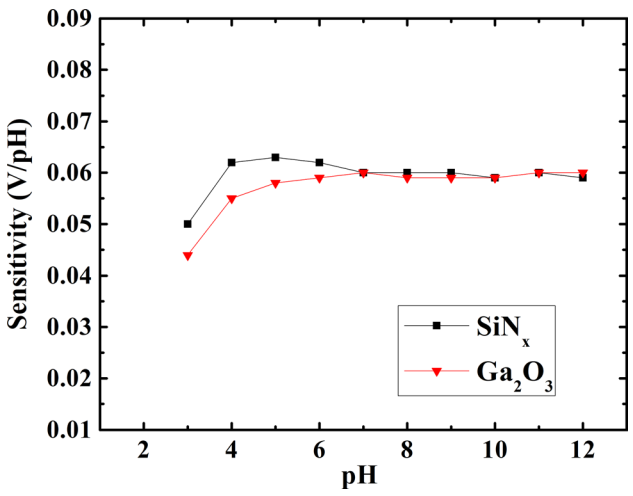

Fig. 4 The variation of the sensitivity with the pH value for devices with SiN_x and Ga_2O_3 passivation layers. The sensitivity is nearly equal to the Nernstian response of 0.59 V/pH

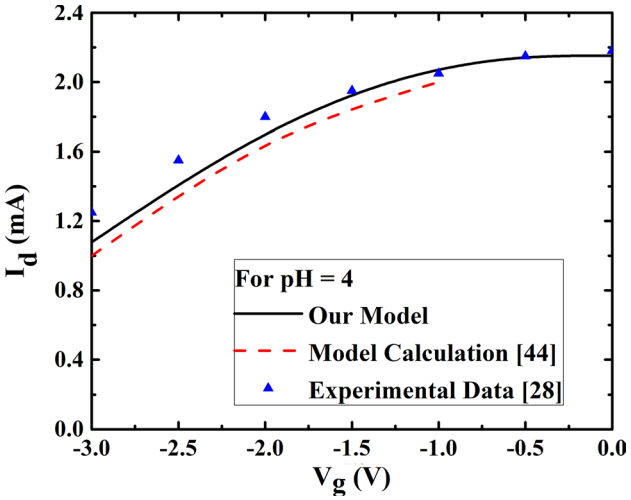

Fig. 5 The I_d–V_g characteristics with $V_{ds} = 0.2$ V at pH 4 for device 2, showing a comparison of the data calculated using our model or that described in Ref. [44] with the experimental data in Ref. [28]. The continuous lines represent the data calculated using our model, the dashed line represents the theoretical calculations of Ref. [44], while the solid triangles represent the experimental data from Ref. [28]

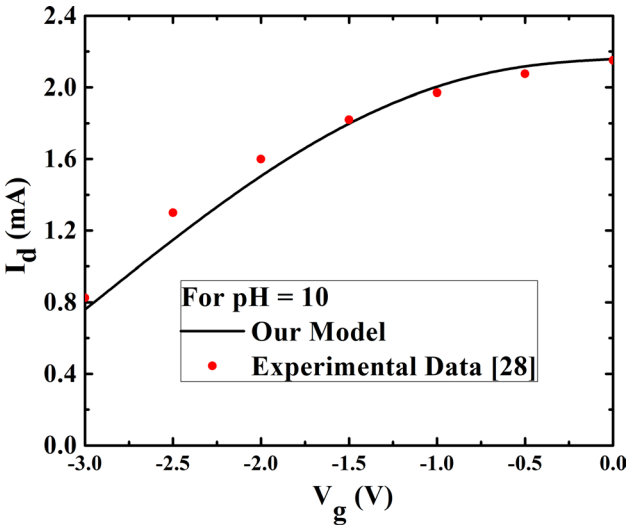

Fig. 6 The I_d–V_g characteristics with $V_{ds} = 0.2$ V at pH 10 for device 2, showing the comparison of the data calculated using our model with the experimental data from Ref. [28]. The lines represent our calculated values, while the solid dots denote the experimental data

for gate voltages above −1.5 V. The minor variations seen below this voltage level may be due to undefined parameters such as the source and drain resistances. Also, some of this mismatch can be attributed to the Schottky barrier height at the metal–AlGaN interface, which may differ depending on the type and quality of the ohmic contact formed by various processes [49]. The units of current in the plots of the drain–current characteristics are different in Figs. 5 and 6 to

enable a comparison of the results calculated herein with the experimental data available in literature.

Figures 7 and 8 show the I_d–V_d characteristics of device 3, which is a bare AlGaN HEMT with an electrolyte solution at pH 1.7 or 11.9. The gate voltages are kept at 0 V and −2 V for both curves. As discussed above, bare AlGaN is covered with Ga_2O_3 when exposed to air. The calculations therefore adopt the parameters for Ga_2O_3. This HEMT has a 25-nm-thick AlGaN layer with an Al content of 25%. The gate width and gate length are fixed at 490 and 40 µm, respectively. The good match with the experiment results of Abidin et al. [24] seen in Figs. 7 and 8 validates the model presented herein. It is also observed that the surface potential decreases with increasing pH value of the electrolyte. This causes a decrease in the drain current of the device. The slight mismatch observed at higher drain voltages between our calculated results and the experimental data in Figs. 7 and 8 may be due to self-heating effects, which are not incorporated herein.

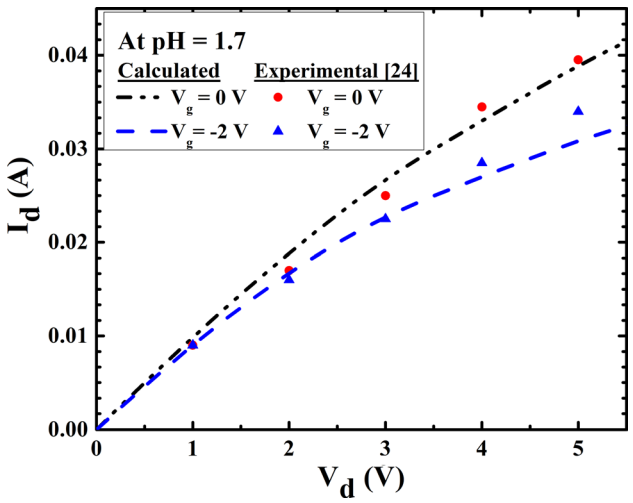

Fig. 7 The drain current I_d and drain voltage V_d characteristics of HEMT device 3 at pH 1.7, showing a comparison of the data calculated using the current model versus the experimental data from Ref. [24] at gate voltages of 0 V and −2 V

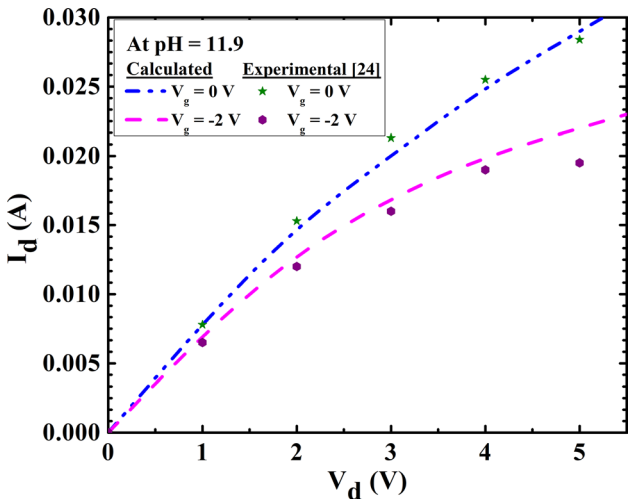

Fig. 8 The drain current I_d and drain voltage V_d characteristics of HEMT device 3 at pH 11.9, showing a comparison of the data calculated using the current model with the experimental data from Ref. [24] at gate voltages of 0 V and −2 V

Figure 9 depicts the value of the effective threshold voltage calculated using Eq. (14) for devices 2 and 3 with electrolyte solutions of different pH values. The effective threshold is calculated by subtracting the surface potential ψ_0 (Eq. 13) from the threshold voltage (Eq. 3). As observed in Fig. 3, the surface potential decreases with increasing pH value, resulting in a shift of the effective threshold value towards positive values.

The evaluation of the best-performing model relies on measurement error analysis [50]. The root-mean-square error (RMSE) is the most widely reported measurement error analysis parameter, representing the sample standard deviation of the calculated and experimental values. Due to the squaring criterion in the RMSE, larger errors have a greater impact on the MSE than do smaller errors. The mean absolute error (MAE) is the most natural and unambiguous measure of the average error magnitude, reporting the closeness of the prediction to the subsequent results [51]. To describe the average model performance error, we calculate the RMSE, MAE, and normalized RMSE (NRMSE) and summarize them in Tables 3, 4, and 5.

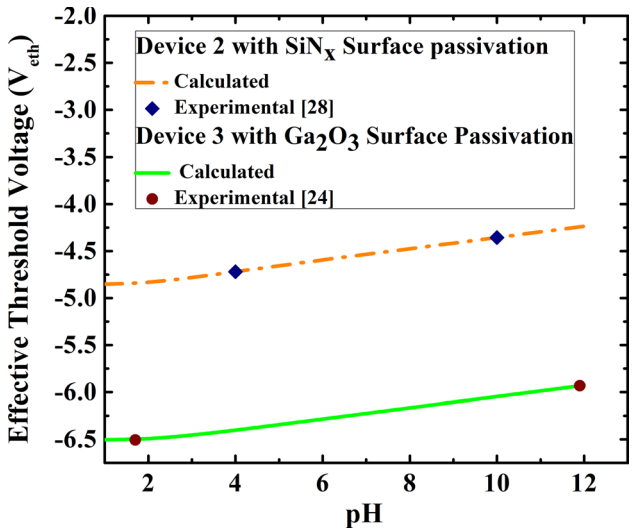

Fig. 9 The change in the effective threshold voltage of the AlGaN/GaN HEMT with variation in the pH value, showing a comparison of the data calculated using the present model for devices 2 and 3 versus the experimental data from Ref. [28] and Ref. [24], respectively. The straight and dashed lines show the calculated results, while the solid symbols denote the experimental values

The RMSE, NRMSE, and MAE values for the I_d–V_g characteristics of devices 1 and 2 at different pH levels are evaluated and summarized in Tables 3 and 4, respectively, revealing that the RMSE of the model proposed herein is 0.053 at pH 4. This is significantly better than result obtained using the basic model by Rabbaa et al. [44] with an RMSE value of 0.166 at the same pH level. Similarly, the NRMSE and MAE values of our model verify the closeness of the values calculated herein to the experimental results, as compared with the results in Ref. [44]. The difference between the results calculated using the model in Ref. [44] and the model presented herein is given in Table 4.

Table 5 summarizes the error measurement for the I_d–V_d characteristics with respect to the experimental results reported in Ref. [24]. The RMSE values presented in Table 5 show the variation due to squaring of larger and smaller errors, while the MAE is constant at 0.001 for the different datasets at different pH levels, thereby demonstrating the reliability of the model presented herein.

Table 3 The RMSE values for our model calculations with respect to the experimental data [48] for the I_d–V_g characteristics of device 1

V_g	Error in I_d
−2	−0.01
−1.5	0.006
−1	−0.003
−0.5	−0.005
0	0
0.5	0.004
1	0.007
1.5	0.019
2	0.02
RMSE	0.0099
NRMSE	0.033
MAE	0.007

Table 5 The RMSE values for the I_d–V_d characteristics of device 3 with solutions at different pH levels

V_d (V)	Error in I_d versus the experimental results in Ref. [24]			
	With solution pH 1.7		With solution pH 11.9	
	At V_g = 0 V	At V_g = −2 V	At V_g = 0 V	At V_g = −2 V
1	0.001	0.00023	0.00011	0.0006
2	0.002	0.001	−0.0003	0.001
3	0.002	0.0005	−0.0013	0.001
4	−0.0015	−0.0015	−0.0005	0.001
5	−0.0005	−0.003	0.0006	0.0025
RMSE	0.0015	0.0015	0.0007	0.0013
NRMSE	0.061	0.072	0.035	0.095
MAE	0.001	0.001	0.001	0.001

5 Conclusions

A new analytical model for the I_d–V_d characteristics of an AlGaN/GaN HEMT for pH sensing is proposed. The impact of the pH of the electrolyte on the drain current, threshold voltage, and surface potential is examined. The voltage in the gate area is indirectly applied as a function of the ionic concentration. The results demonstrate that, by applying an SiN_x passivation layer to the HEMT, the sensitivity at lower pH values is improved. The current analytical results show good agreement with experimental results available in literature. The overall average RMSE value of our model is 0.018 for the I_d–V_d characteristics of different devices, with and without the solution pH. This error range is within

Table 4 The RMSE values for the $I_d - V_g$ characteristics of device 2 with solutions at different pH levels

V_g (V)	Difference in I_d when calculated using the model in Ref. [44] versus the current model	Error when using the current model to calculate I_d versus the experimental results in Ref. [28]		Error when using the model in Ref. [44] to calculate I_d versus the experimental results in Ref. [28]
	With solution pH 4	With solution pH 4	With solution pH 10	With solution pH 4
−3	−0.078	−0.072	0.065	−0.25
−2.5	−0.063	−0.067	0.097	−0.2
−2	−0.059	−0.091	0.085	−0.15
−1.5	−0.086	−0.014	0.007	−0.1
−1	−0.084	0.034	−0.049	−0.05
−0.5	–	0.003	−0.056	–
0	–	−0.028	–0.008	–
RMSE	–	0.053	0.061	0.166
NRMSE	–	0.03	0.037	0.106
MAE	–	0.044	0.052	0.15

acceptable physical limits. Some limitations were identified at higher drain voltages, where the calculated and experimental values differ in the I_d–V_d characteristics. This can be attributed to second-order effects such as short-channel effects (SCE) and self-heating effects (SHE), which are not included in the presented model. SCEs, SHEs, and illumination effects will be included in an extended version of this model in the future.

In summary, the current model exhibits smaller errors and is simpler and more reliable than other models available in the literature. To the best of the authors' knowledge, no such *I*–*V* model has been specifically implemented for pH sensing applications. In conclusion, the current model will have significant applications for device optimization and standardization of prospective chemical and biosensors.

References

1. Sawant, R.M., Hurley, J.P., Salmaso, S., Kale, A., Tolcheva, E., Levchenko, T.S., Torchilin, V.P.: SMART drug delivery systems: double-targeted pH-responsive pharmaceutical nanocarriers. Bioconjugate Chem. **17**(4), 943–949 (2006)
2. Caló, E., Khutoryanskiy, V.V.: Biomedical applications of hydrogels: A review of patents and commercial products. Eur. Polym. J. **65**, 252–267 (2015)
3. Bousse, L., De Rooij, N.F., Bergveld, P.: Operation of chemically sensitive field-effect sensors as a function of the insulator electrolyte interface. IEEE Trans. Electron Devices **ED-30**(10), 1263–1270 (1983)
4. Chiang, J.L., Chen, Y.C., Chou, J.C.: Simulation and experimental study of the pH-sensing property for AlN thin films. Jpn. J. Appl. Phys. **40**(10), 5900–5904 (2001)
5. Mahabadi, S.J., Moghadam, H.A.: Comprehensive study of a 4H–SiC MES–MOSFET. Phys. E Low-Dimens. Syst. Nanostruct. **74**, 25–29 (2015)
6. Moghadam, H.A., Dimitrijev, S., Han, J., Haasmann, D., Aminbeidokhti, A.: Transient-current method for measurement of active near-interface oxide traps in 4H-SiC MOS capacitors and MOSFETs. IEEE Trans. Electron Devices **62**(8), 2670–2674 (2015)
7. Holmes, J., Dutta, M., Koeck, F.A., Benipal, M., Brown, J., Fox, B., Hathwar, R., Johnson, H., Malakoutian, M., Saremi, M., Zaniewski, A.: A 4.5-μm PIN diamond diode for detecting slow neutrons. Nucl. Instrum. Methods Phys. Res. Sect A Accel. Spectrom. Detectors Assoc. Equip. **903**, 297–301 (2018)
8. Saremi, M., Hathwar, R., Dutta, M., Koeck, F.A., Nemanich, R.J., Chowdhury, S., Goodnick, S.M.: Analysis of the reverse I-V characteristics of diamond-based PIN diodes. Appl. Phys. Lett. **111**(4), 043507 (2017)
9. Saremi, M.: Modeling and simulation of the programmable metallization cells (PMCs) and diamond-based power devices. Doctoral Dissertation, Arizona State University, (2017).
10. Hassan, A., Savaria, Y., Sawan, M.: GaN integration technology, an ideal candidate for high-temperature applications: a review. IEEE Access **6**, 78790–78802 (2018)
11. Alexandru, M., Banu, V., Jordà, X., Montserrat, J., Vellvehi, M., Tournier, D., Millán, J., Godignon, P.: SiC integrated circuit control electronics for high-temperature operation. IEEE Trans. Ind. Electron. **62**(5), 3182–3191 (2015)
12. Gaska, R., Gaevski, M., Jain, R., Deng, J., Islam, M., Simin, G., Shur, M.: Novel AlInN/GaN integrated circuits operating up to 500 C. Solid-State Electron. **113**, 22–27 (2015)
13. Chaniotakis, N., Sofikiti, N.: Novel semiconductor materials for the development of chemical sensors and biosensors: a review. Anal. Chim. Acta **615**(1), 1–9 (2008)
14. Upadhyay, K.T., Chattopadhyay, M.K.: Sensor applications based on AlGaN/GaN heterostructures. Mater. Sci. Eng. B **263**, 114849 (2021)
15. Pearton, S.J., Ren, F., Zhang, A.P., Dang, G., Cao, X.A., Lee, K.P., Cho, H.: GaN electronics for high power, high temperature applications. Mater. Sci. Eng. B **82**(1–3), 227–231 (2001)
16. Dong, Y., Son, D., Dai, Q., Lee, J., Won, C., Kim, J., Kang, S., Lee, J., Chen, D., Lu, H., Zhang, R., Zheng, Y.: AlGaN/GaN heterostructure pH sensor with multi-sensing segments. Sensors Actuators B Chem. **260**, 134–139 (2018)
17. Heinz, D., Huber, F., Spiess, M., Asad, M., Wu, L.Y., Rettig, O.: GaInN quantum wells as optochemical transducers for chemical sensors and biosensors. IEEE J. Sel. Top. Quantum Electron. **23**, 15–23 (2017)
18. Kushagra, A., Pradhan, A.K., Bazal, D.: pH-dependent electrochemomechanical transition of hydrophobe-water interface. IEEE Sensors Lett. **3**(7), 1–4 (2019)
19. Yates, D.E., Levine, S., Healy, T.W.: Site-binding model of the electrical double layer at the oxide/water interface. J. Chem. Soc. Faraday Trans. 1 Phys Chem. Condens. Phases **70**, 1807–1818 (1974)
20. Mönch, W.: Elementary calculation of the branch-point energy in the continuum of interface-induced gap states. Appl. Surf. Sci. **117–118**, 380–387 (1997)
21. Steinhoff, G., Hermann, M., Schaff, W.J., Eastman, L.F., Stutzmann, M., Eickhoff, M.: *p*H response of GaN surfaces and its application for *p*H-sensitive field-effect transistors. Appl. Phys. Lett. **83**(1), 177–179 (2003)
22. Schubert, T., Steinhoff, G., Ribbeck, H.-G.V., Stutzmannn, M., Eickhoff, M., Tanaka, M.: Gallium nitride electrodes for membrane-based electrochemical biosensors. Eur. Phys. J. E **30**(2), 233–238 (2009)
23. Cimalla, I.: AlGaN/GaN Sensors for Direct Monitoring of Fluids and Bioreactions. Universitätsverlag Ilmenau, Ilmenau (2011). https://www.db-thueringen.de/receive/dbt_mods_00018484
24. Abidin, M.S.Z., Hashim, A.M., x Sharifabad, A.M., Rahman, S.F., Sadoh, T.: Open-gated pH sensor fabricated on an undoped-AlGaN/GaN HEMT structure. Sensors **11**(3), 77–3067 (2011)
25. Pyo, J.Y., Jeon, J.H., Koh, Y., Cho, C.Y., Park, H.H., Park, K.H., Lee, S.W., Cho, W.J.: AlGaN/GaN high-electron-mobility transistor pH sensor with extended gate platform. AIP Adv. **8**(8), 085106 (2018)
26. Stutzmann, M., Steinhoff, G., Eickhoff, M., Ambacher, O., Nebel, C.E., Schalwig, J., Neuberger, R., Müller, G.: GaN-based heterostructures for sensor applications. Diamond Relat. Mater. **11**(3–6), 886–891 (2002)
27. Mehandru, R., Luo, B., Kang, B.S., Kim, J.H., Ren, F., Pearton, S.J., Chyi, J.I.: AlGaN/GaN HEMT based liquid sensors. Solid-State Electron. **48**(2), 351–353 (2004)
28. Kokawa, T., Sato, T., Hasegawa, H., Hashizume, T.: Liquid-phase sensors using open-gate AlGaN/GaN high electron mobility transistor structure. J. Vacuum Sci. Technol. B Microelectron. Nanometer. Struct. Process Meas. Phenom. **24**(4), 1972–1976 (2006)
29. Sharma, N., Mishra, S., Singh, K., Chaturvedi, N., Chauhan, A., Periasamy, C., Kharbanda, D.K., Parjapat, P., Khanna, P.K., Nidhi, C.: High-resolution AlGaN/GaN HEMT-based electrochemical sensor for biomedical applications. IEEE Trans. Electron Devices **67**(1), 289–295 (2020)
30. Cheng, Q., Wang, M., Tao, M., Yin, R., Li, Y., Yang, N., Xu, W., Gao, C., Hao, Y., Yang, Z.: Planar dual gate GaN HEMT cascode

amplifier as a voltage readout pH sensor with high and tunable sensitivities. IEEE Electron Device Lett. **41**(3), 485–488 (2020)
31. Xuea, D., Zhanga, H., Ahmada, A.U., Lianga, H., Liua, J., Xiaa, X., Guob, W., Huangc, H., Xu, N.: Enhancing the sensitivity of the reference electrode free AlGaN/GaN HEMT based pH sensors by controlling the threshold voltage. Sensors Actuators B. Chem. **306**, 127609 (2020)
32. Zhang, H., Tub, J., Yanga, S., Sheng, K., Wang, P.: Optimization of gate geometry towards high-sensitivity AlGaN/GaN pH sensor. Talanta **205**, 120134 (2019)
33. Chattopadhyay, M.K., Tokekar, S.: Temperature and polarization dependent polynomial based non-linear analytical model for gate capacitance of AlmGa1−mN/GaN MODFET. Solid-State Electron. **50**, 2 (2006)
34. Sadi, T., Frank, S.: A continuous physics-based electro-thermal compact model for the study of non-linearities in III–V HEMTs. In: IEEE European Solid State Device Research Conf; (2010).
35. Rudolph, M., Fager, C., Root, D.E.: Non-linear Transistor Parameter Extraction Technique. Cambridge University Press, Cambridge (2012)
36. Koudymov, A., Shur, M.S., Simin, G., Chu, K., Chao, P.C., Lee, C.: Analytical HFET I-V model in presence of current collapse. IEEE Trans Electron Dev. **55**(3), 712–720 (2008)
37. Miao, L., Wang, Y.: 2-D analytical model for current–voltage characteristics and transconductance of AlGaN/GaN MODFETs. IEEE Trans. Electron Dev. **55**(1), 261–267 (2008)
38. Cheng, X., Li, M., Wang, Y.: Physics based compact model for AlGaN/GaN MODFET with closed form I-V and C–V characteristics. IEEE Trans. Electron Dev. **56**(12), 288–2887 (2009)
39. Kola, S., Golio, J.M., Maracas, G.N.: An analytical expression for Fermi Level versus sheet carrier concentration for HEMT modeling. IEEE Electron Dev. Lett. **9**, 136–138 (1988)
40. John, D.L., Allerstam, F., Rodle, T., Murad, S. K., Smit, GDJ.: A surface-potential based model for GaN HEMT in RF power amplifier applications. In: IEEE International Electron Device Meeting (IEDM); (2010).
41. Khandelwal, S., Fjeldly, T.A.: A physics based compact model of I-V and C–V characteristics in AlGaN/GaN HEMT devices. Solid-State Electron. **76**, 60–66 (2012)
42. Karumuri, N., Turuvekere, S., Gupta, N.D., Gupta, A.D.: A continuous analytical model for 2-DEG charge density in AlGaN/GaN HEMTs valid for all bias voltages. IEEE Trans. Electron Devices **61**(7), 2343–2349 (2014)
43. Swamy, N.S., Dutta, A.K.: Analytical models for the 2DEG density, AlGaN layer carrier density, and drain current for AlGaN/GaN HEMTs. IEEE Trans. Electron Devices **65**(3), 936–944 (2018)
44. Rabbaa, S., Stiens, J.: Validation of a triangular quantum well model for GaN-based HEMTs used in pH and dipole moment sensing. J. Phys. D Appl. Phys. **45**(47), 475101 (2012)
45. Upadhyay, K.T., Chattopadhyay, M.K.: Al composition and $Al_xIn_yGa_zN$ layer thickness dependent new analytical model for IV characteristics of AlxInyGazN/GaN HEMTs. Mater. Today Proc. **19**, 205–208 (2019)
46. Yigletu, F.M., Khandelwal, S., Fjeldly, T.A., Benjamín, I.: Compact charge-based physical models for current and capacitances in AlGaN/GaN HEMTs. IEEE Trans. Electron Devices **60**(11), 3746–3752 (2013)
47. Narang, R., Saxena, M., Gupta, M.: Analytical model of pH sensing characteristics of junctionless silicon on insulator ISFET. IEEE Trans. Electron Devices **64**(4), 1742–1750 (2017)
48. Wu, Y.-F., Keller, S., Kozodoy, P., Keller, B.P., Parikh, P., Kapolnek, D., Denbaars, S.P., Mishra, U.K.: Bias dependent microwave performance of AlGaN/GaN MODFET's up to 100 V. IEEE Electron Device Lett. **18**(6), 290–292 (1997)
49. Wang, Y.H., Liang, Y.C., Samudra, G.S., Chang, T., Huang, C., Yuan, L., Lo, G.: Modelling temperature dependence on AlGaN/GaN power HEMT device characteristics. Semicond. Sci. Technol. **28**(12), 125010 (2013)
50. Pal, R.: Predictive Modeling of Drug Sensitivity, pp. 83–104. Academic, Cambridge (2016)
51. Willmott, C.J., Matsuura, K.: Advantages of the mean absolute error (MAE) over the root mean square error (RMSE) in assessing average model performance. Climate Res **30**(1), 79–82 (2005)

Terms and Conditions

Springer Nature journal content, brought to you courtesy of Springer Nature Customer Service Center GmbH (“Springer Nature”).
Springer Nature supports a reasonable amount of sharing of research papers by authors, subscribers and authorised users (“Users”), for small-scale personal, non-commercial use provided that all copyright, trade and service marks and other proprietary notices are maintained. By accessing, sharing, receiving or otherwise using the Springer Nature journal content you agree to these terms of use (“Terms”). For these purposes, Springer Nature considers academic use (by researchers and students) to be non-commercial.
These Terms are supplementary and will apply in addition to any applicable website terms and conditions, a relevant site licence or a personal subscription. These Terms will prevail over any conflict or ambiguity with regards to the relevant terms, a site licence or a personal subscription (to the extent of the conflict or ambiguity only). For Creative Commons-licensed articles, the terms of the Creative Commons license used will apply.
We collect and use personal data to provide access to the Springer Nature journal content. We may also use these personal data internally within ResearchGate and Springer Nature and as agreed share it, in an anonymised way, for purposes of tracking, analysis and reporting. We will not otherwise disclose your personal data outside the ResearchGate or the Springer Nature group of companies unless we have your permission as detailed in the Privacy Policy.
While Users may use the Springer Nature journal content for small scale, personal non-commercial use, it is important to note that Users may not:

1. use such content for the purpose of providing other users with access on a regular or large scale basis or as a means to circumvent access control;
2. use such content where to do so would be considered a criminal or statutory offence in any jurisdiction, or gives rise to civil liability, or is otherwise unlawful;
3. falsely or misleadingly imply or suggest endorsement, approval , sponsorship, or association unless explicitly agreed to by Springer Nature in writing;
4. use bots or other automated methods to access the content or redirect messages
5. override any security feature or exclusionary protocol; or
6. share the content in order to create substitute for Springer Nature products or services or a systematic database of Springer Nature journal content.

In line with the restriction against commercial use, Springer Nature does not permit the creation of a product or service that creates revenue, royalties, rent or income from our content or its inclusion as part of a paid for service or for other commercial gain. Springer Nature journal content cannot be used for inter-library loans and librarians may not upload Springer Nature journal content on a large scale into their, or any other, institutional repository.
These terms of use are reviewed regularly and may be amended at any time. Springer Nature is not obligated to publish any information or content on this website and may remove it or features or functionality at our sole discretion, at any time with or without notice. Springer Nature may revoke this licence to you at any time and remove access to any copies of the Springer Nature journal content which have been saved.
To the fullest extent permitted by law, Springer Nature makes no warranties, representations or guarantees to Users, either express or implied with respect to the Springer nature journal content and all parties disclaim and waive any implied warranties or warranties imposed by law, including merchantability or fitness for any particular purpose.
Please note that these rights do not automatically extend to content, data or other material published by Springer Nature that may be licensed from third parties.
If you would like to use or distribute our Springer Nature journal content to a wider audience or on a regular basis or in any other manner not expressly permitted by these Terms, please contact Springer Nature at

onlineservice@springernature.com